



Instrument-model refinement in normalized reciprocal-vector space for X-ray Laue diffraction

Radosław Kamiński, Dariusz Szarejko, Martin N. Pedersen, Lauren E. Hatcher, Piotr Łaski, Paul R. Raithby, Michael Wulff and Katarzyna N. Jarzemska

J. Appl. Cryst. (2020). **53**, 1370–1375



IUCr Journals
CRYSTALLOGRAPHY JOURNALS ONLINE

Copyright © International Union of Crystallography

Author(s) of this article may load this reprint on their own web site or institutional repository provided that this cover page is retained. Republication of this article or its storage in electronic databases other than as specified above is not permitted without prior permission in writing from the IUCr.

For further information see <https://journals.iucr.org/services/authorrights.html>



Instrument-model refinement in normalized reciprocal-vector space for X-ray Laue diffraction

Radostaw Kamiński,^{a*} Dariusz Szarejko,^a Martin N. Pedersen,^b Lauren E. Hatcher,^{c,d} Piotr Łaski,^a Paul R. Raithby,^c Michael Wulff^e and Katarzyna N. Jarzemska^{a*}

Received 3 May 2020

Accepted 29 August 2020

Edited by J. Hajdu, Uppsala University, Sweden and The European Extreme Light Infrastructure, Czech Republic

Keywords: data processing; Laue diffraction; instrument models; refinement; X-ray diffraction.

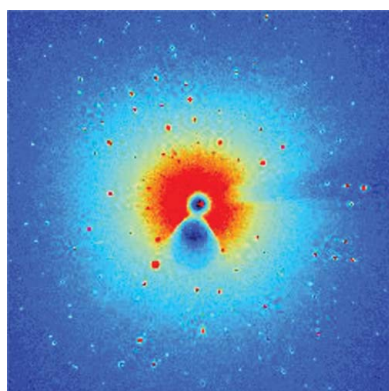
Supporting information: this article has supporting information at journals.iucr.org/j

^aDepartment of Chemistry, University of Warsaw, Żwirki i Wigury 101, 02-089 Warsaw, Poland, ^bNiels Bohr Institute, University of Copenhagen, Universitetsparken 5, 2100 Copenhagen, Denmark, ^cDepartment of Chemistry, University of Bath, Claverton Down, Bath BA2 7AY, United Kingdom, ^dSchool of Chemistry, Cardiff University, Main Building, Park Place, Cardiff CF10 3AT, United Kingdom, and ^eEuropean Synchrotron Radiation Facility, 71 avenue des Martyrs, 38043 Grenoble, France. *Correspondence e-mail: rkaminski85@uw.edu.pl, katarzyna.jarzemska@uw.edu.pl

A simple yet efficient instrument-model refinement method for X-ray diffraction data is presented and discussed. The method is based on least-squares minimization of differences between respective normalized (*i.e.* unit length) reciprocal vectors computed for adjacent frames. The approach was primarily designed to work with synchrotron X-ray Laue diffraction data collected for small-molecule single-crystal samples. The method has been shown to work well on both simulated and experimental data. Tests performed on simulated data sets for small-molecule and protein crystals confirmed the validity of the proposed instrument-model refinement approach. Finally, examination of data sets collected at both BioCARS 14-ID-B (Advanced Photon Source) and ID09 (European Synchrotron Radiation Facility) beamlines indicated that the approach is capable of retrieving goniometer parameters (*e.g.* detector distance or primary X-ray beam centre) reliably, even when their initial estimates are rather inaccurate.

1. Introduction

Studies of short-lived light-induced excited states in crystals of small molecules are currently feasible almost exclusively at high-intensity X-ray sources, such as synchrotrons (Hatcher & Raithby, 2014; Coppens, 2011; Coppens *et al.*, 2010). In this regard, the time-resolved (TR) X-ray diffraction Laue method, applied originally for macromolecular samples (Ren *et al.*, 1999; Hajdu *et al.*, 1987), constitutes the most efficient approach, as it allows effectively single-pulse diffraction experiments thanks to a high X-ray flux. However, data processing in the case of a polychromatic X-ray beam is considerably more difficult than the monochromatic approach (Coppens & Fournier, 2015). Among other factors, this is caused by a number of wavelength-dependent corrections which have to be applied. Such problems can be significantly reduced by employing the RATIO method (Coppens *et al.*, 2009), in which the Laue experiment provides only light-ON to light-OFF reflection intensity ratios ($I^{\text{ON}}/I^{\text{OFF}}$). These in turn are further analysed so as to obtain electron-density photodifference maps and later structural models of transient species (Trzop *et al.*, 2014; Jarzemska *et al.*, 2014, 2019; Makal *et al.*, 2012; Benedict *et al.*, 2011; Coppens *et al.*, 2017; Vorontsov *et al.*, 2010). Consequently, the data processing pipeline concentrates here on the integration of diffraction spots (Kalinowski *et al.*, 2012; Szarejko *et al.*, 2020) and crystal orientation-matrix determination. For small-molecule crystals



the latter step is most efficiently achieved with the algorithm proposed by Kalinowski *et al.* (2011) and implemented in the *LaueUtil* software. Nevertheless, the success of this approach depends heavily on an appropriate description of the goniometer geometry used, described with a mathematical instrument model (IM) including parameters of the experimental setup (*e.g.* detector distance, detector size and position, goniostat zeros *etc.*) (Paciorek *et al.*, 1999). Therefore, in more difficult cases, where sufficiently accurate instrument-model parameters are not available (an inaccurate IM is quite common on a busy user-operated synchrotron beamline, where equipment is regularly moved or exchanged depending on different user requirements *etc.*), the entire data processing is significantly hampered (if it is possible at all), since the *LaueUtil* suite does not have capabilities either to determine or to refine the IM. This option is provided, for example, in the *PRECOGNITION* suite (Šrajer *et al.*, 2000), which, however, is not open source and is not fully optimized for small-molecule crystals where sparse diffraction patterns are observed. Such cases require the collection of a reference data set on a known protein crystal standard (*e.g.* photoactive yellow protein, PYP; Borgstahl *et al.*, 1995) prior to actual experiments. In cases where such reference data are not available, the data processing is much more problematic. Hence, to fill this gap, in the current short contribution a simple yet efficient *ab initio* method to refine instrument-model parameters is reported. Importantly, the algorithm relies only on diffraction spot positions and does not require an orientation matrix, wavelength spectrum *etc.*

2. Results and discussion

A typical Laue X-ray diffraction experiment performed for a single-crystal sample is depicted schematically in Fig. 1(a). Diffraction images (*i.e.* frames) are usually collected for a sample being kept still (*i.e.* not rotated during the exposure), since it is possible to record full reflections using a polychromatic X-ray beam. This feature of the method allows it to be employed efficiently for time-resolved X-ray diffraction studies. In this contribution we assume the simplest case of a Laue experiment, in which a total of N frames (*e.g.* 90 or 180 frames) are collected during sample rotation along a single-spindle axis, each at a different sample orientation separated from the adjacent one by some angular interval, $\Delta\varphi$ (*e.g.* 1 or 2°). Fig. 1(b) shows how selected diffraction spots change position on the detector surface when the crystal is rotated along the horizontal axis. Furthermore, we assume that the sample is firmly attached to the holder (*e.g.* it is glued), and thus no irregular sample movements are present.

Since in the Laue method a polychromatic X-ray beam is diffracted by a single-crystal sample, assigning a specific wavelength to a given recorded single diffraction spot is not initially straightforward. Thus, before the orientation-matrix and indexing data processing steps, reconstruction of the reciprocal space is not feasible. (We note that such procedures are much easier when the unit-cell parameters are known *a priori* but become more cumbersome in the case of sparse

diffraction patterns.) Nonetheless, it is possible to compute normalized (*i.e.* unit-length) reciprocal-space vectors, $\tilde{\mathbf{h}}$, as proposed by Kalinowski *et al.* (2011):

$$\tilde{\mathbf{h}} = \frac{\mathbf{s} - \mathbf{s}_0}{\|\mathbf{s} - \mathbf{s}_0\|}, \quad (1)$$

where \mathbf{s} and \mathbf{s}_0 are the diffracted and primary beams' unit-length vectors, respectively. The $\tilde{\mathbf{h}}$ vectors are subsequently appropriately rotated (using goniometer setting angles known for each frame) to a common goniometer-head-fixed coordinate system (with all goniometer angles equal to zero), yielding a unit-sphere-projected set of vectors (denoted here as $\tilde{\mathbf{h}}_0$ for convenience) for the entire data set [for visualization see, for example, Fig. 1(b) of Kalinowski *et al.* (2011)]. Computation of the $\tilde{\mathbf{h}}_0$ vectors from spot positions on the detector surface requires knowledge of the instrument-model parameters. Thus each vector of this kind is a function of those parameters (for details see the supporting information).

During analysis of the available TR Laue data sets, it appeared that, despite using approximate IM parameters (*e.g.* detector distance is off by several millimetres), most of the $\tilde{\mathbf{h}}_0$ vectors computed for reflections with the same hkl indices present in adjacent frames are very similar to one another in terms of direction. For ideal IM parameters, such derived $\tilde{\mathbf{h}}_0$ vectors should overlap (this is schematically shown in Fig. 2, in which two selected pairs of $\tilde{\mathbf{h}}_0$ vectors computed for adjacent frames are presented). This fact constitutes the basis for our refinement procedure. The $\tilde{\mathbf{h}}_0$ vectors computed for the adjacent frames are first paired using a simple geometrical criterion (*i.e.* the angular separation). The sum of difference vector lengths in these pairs,

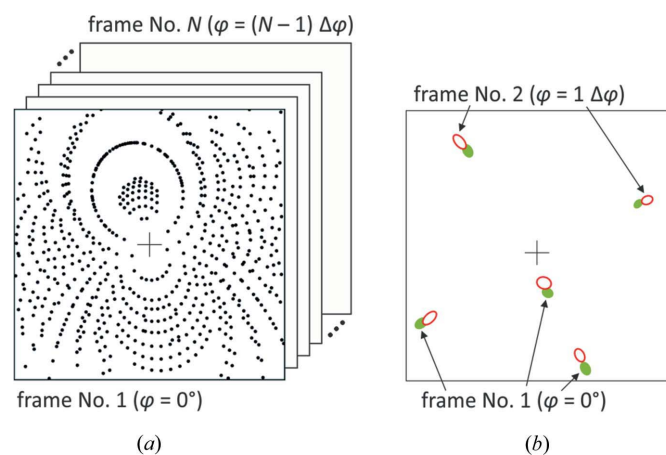


Figure 1
(a) Schematic representation of a typical Laue data set consisting of diffraction frames measured at various goniometer setting angles (*i.e.* each frame is collected with the sample rotated by a certain increment, $\Delta\varphi$). A single φ -angle spindle axis is assumed for simplicity. This example data set consists of N frames; the cross indicates the frame's centre. (b) Overlay of two adjacent frames showing changes in the positions of selected spots due to the horizontal sample rotation ($\Delta\varphi = 1^\circ$): green solid spots – frame No. 1, red empty spots – frame No. 2 (for an overlay of two frames see the supporting information; displacements, spot sizes and shapes are exaggerated).

$$S = \sum_{j=1}^{N-1} \sum_{k(j)} \|\tilde{\mathbf{h}}_{0,k,j} - \tilde{\mathbf{h}}_{0,k,j+1}\|^2, \quad (2)$$

is then least-squares minimized with respect to the chosen instrument-model parameters, starting from some initial estimated values (e.g. an approximate detector distance). Here j and k denote frames and vector pairs found for two adjacent frames; the j index runs from 1 to $N - 1$ for a data set with N frames. Note that the number of determined reflection pairs is different for various pairs of adjacent frames.

In our simple IM only three parameters are considered crucial for further data analysis with the RATIO method, namely the detector distance, and the horizontal and vertical primary beam positions on the detector surface: d , x_0 and y_0 , respectively. It is assumed that the detector is placed ideally perpendicularly at $2\theta = 0^\circ$ with respect to the primary beam and there are no further goniometer misalignments. More details on the instrument model, used definitions, equations and implementation comments are available in the supporting information.

The algorithm was tested on a couple of model simulated and experimental data sets. The refinement of the instrument model on simulated X-ray Laue diffraction data sets for two crystal structures, namely a small-molecule compound, $\text{Ag}_2\text{Cu}_2\text{L}_4$ ($L = 2$ -diphenylphosphino-3-methylindole) (Koshvoy *et al.*, 2011), and a pea lectin protein (Einspahr *et al.*, 1986), constituted the primary benchmark. The silver(I)-copper(I) tetranuclear complex was studied by us using both TR Laue diffraction and high-pressure crystallography (triclinic space group $P\bar{1}$) (Jarzemska *et al.*, 2014, 2018). The pea lectin protein crystal structure was studied extensively with Laue diffraction by Helliwell and co-workers (orthorhombic space group $P2_12_12_1$) (Cruickshank *et al.*, 1987, 1991; Helliwell *et al.*, 1989; Machin, 1985). The simulated models account only for the diffraction geometry and not diffraction

spot intensities (for details see the supporting information). To cover this aspect, experimental data sets of high quality collected for two copper(I) complexes are used as two further test cases. The first one, $\text{Cu}(\text{dppe})(\text{dmp})\text{PF}_6$ [dppe = 1,2-bis-(diphenylphosphino)ethane, dmp = 2,9-dimethyl-1,10-phenanthroline] (monoclinic space group $P2_1/c$), was studied previously by Voronstov *et al.* (2009) using the monochromatic TR technique and later by us using both Laue and in-house TR diffraction methods (Trzop *et al.*, 2014; Coppens *et al.*, 2016; Kaminski *et al.*, 2014). The data set used here was measured at the 14-ID-B BioCARS beamline (Graber *et al.*, 2011) at the Advanced Photon Source (APS). The data for the second compound, $\text{Cu}(\text{dppe})(\text{dmdpp})\text{PF}_6$ (dmdpp = 2,9-dimethyl-4,7-diphenyl-1,10-phenanthroline) (monoclinic space group $P2_1/n$), were collected at the ID09 beamline (Wulff *et al.*, 2002) at the European Synchrotron Radiation Facility (ESRF). Both data sets were initially integrated using our new one-dimensional seed-skewness method (Szarejko *et al.*, 2020), which resulted in a set of reflection intensities and positions. All data sets examined in this study are summarized in Table 1, including their abbreviations used hereafter. Examples of simulated and experimental frames are shown in the supporting information.

Results of the instrument-model refinement are shown in Table 2. In the case of simulated data, **simAgCu** and **simPeaL**, the refinements converge very well to the values used in the simulation with estimated standard deviations (e.s.d.s) of the order of 10^{-5} or better (in millimetres or pixels), indicating a nearly perfect fit. It should be stressed that the correct results are obtained even if the detector distance deviates from the real value by more than 1 cm. Therefore, the achieved accuracy is far more than sufficient for real applications, as the initial detector distance can easily be determined to at least 1 mm precision with mechanical tools.

Regarding the data collected at the 14-ID-B beamline at the APS, for **expCuDppe**, the instrument geometry was tested with the PYP crystal and the **PRECOGNITION** software. The primary beam position was determined by collecting its direct image by attenuating X-rays. Therefore, this data set can be used to test the accuracy of our software at reproducing these known parameters. In our software, refinement of the instrument parameters from different starting points (including the detector distance set to as much as 120 mm) yielded essentially identical results, *i.e.* $d = 100.80$ (7) mm instead of the assumed exact value of 100 mm. We believe this is well within experimental error, and thus such a difference is perfectly acceptable. The beam position refined to values that are almost identical to those we measured when the detector was directly exposed to the attenuated primary beam.

In the case of the **expCuDmdpp** data set, collected at the ID09 beamline of the ESRF, we encountered some problems when indexing the measured data using the method of Kalinowski *et*

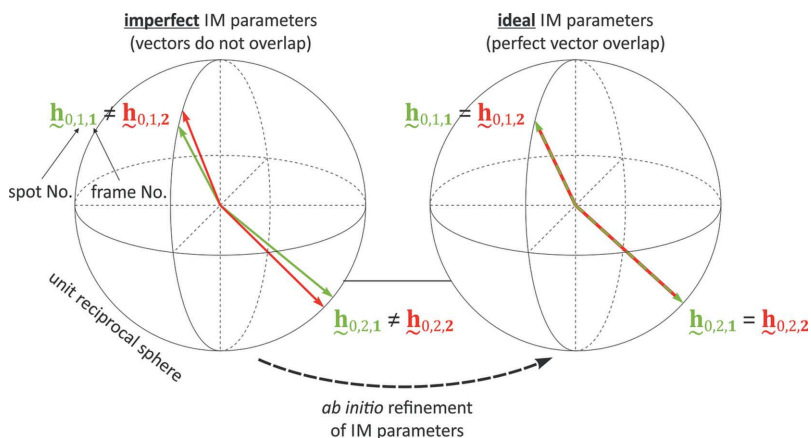


Figure 2

Schematic representation of two selected adjacent-frame pairs of normalized reciprocal vectors $\tilde{\mathbf{h}}_0$ with the same hkl indices [see e.g. Fig. 1(b)] reconstructed from spot positions, goniometer setting angles and other instrument model parameters (e.g. detector distance, primary beam position etc.). Left panel: imperfect IM parameters (the respective vectors do not overlap); right panel: ideal IM parameters (the reconstructed vectors overlap perfectly after the least-squares minimization of vector differences with respect to IM parameters).

Table 1
Selected parameters for simulated and experimental data sets used in this study.

	Simulated data		Experimental data	
	Ag ₂ Cu ₂ L ₄ complex	Pea lectin protein	Cu(dppe)(dmp)PF ₆ complex	Cu(dppe)(dmdpp)PF ₆ complex
Data set abbreviation	simAgCu	simPeaL	expCuDppe	expCuDmdpp
X-ray source	—	—	14-ID-B at APS	ID09 at ESRF
Space group	<i>P</i> $\bar{1}$ (No. 2)	<i>P</i> 2 ₁ 2 ₁ (No. 19) ^a	<i>P</i> 2 ₁ / <i>c</i> (No. 14)	<i>P</i> 2 ₁ / <i>n</i> (No. 14)
<i>a</i> (Å)	12.6106 (2)	50.73 (2)	20.2099 (4)	14.1511 (6)
<i>b</i> (Å)	14.1988 (3)	61.16 (2)	13.6740 (3)	14.2212 (5)
<i>c</i> (Å)	22.0662 (4)	136.59 (8)	26.5809 (5)	27.3870 (10)
α (°)	76.3912 (3)	90	90	90
β (°)	81.5811 (3)	90	95.5178 (2)	98.373 (3)
γ (°)	66.8814 (3)	90	90	90
Detector distance, <i>d</i> (mm)	65.0 ^b	95.0 ^b	100.0 ^c	50.0 ^c
Beam position				
<i>x</i> ₀ (pixels)	19540.0 ^b	1215.0 ^b	19860.0 ^d	19100.0 ^e
<i>y</i> ₀ (pixels)	19730.0 ^b	1286.0 ^b	19640.0 ^d	19240.0 ^e
Detector shape	Square	Square	Square ^f	Square ^g
Detector dimensions (mm) ^h	340.0	120.0 ⁱ	340.0 ^f	170.0 ^g
Frame dimensions (pixels) ^h	3840	2400 ⁱ	3840 ^f	3840 ^g
Pixel size (µm) ^h	89.0	20.0 ⁱ	89.0 ^f	44.0 ^g
Wavelength range				
λ_{\min} (Å)	0.8	0.5	0.8 ^j	0.75 ^j
λ_{\max} (Å)	1.1	2.6	1.1 ^j	1.1 ^j
Number of frames	91	91	91	91
Angular increment, $\Delta\varphi$ (°)	1.0	1.0	1.0	1.0
Angular coverage, φ_{tot} (°)	91.0	91.0	91.0	91.0

Notes: (a) For simplicity, systematic absence conditions are omitted in this contribution. (b) Values used in the simulation. (c) As assumed to be correct in the data collection software. (d) Primary beam position measured with the *ADXV* program (Arvai, 2019) from the reference frame with direct beam image (appropriate filters were used to maximally attenuate the beam). (e) Primary beam position was assumed to be close to the beamstop shadow centre. (f) Rayonix MX340-HS detector mounted at the 14-ID-B BioCARS beamline at the APS (Graber *et al.*, 2011). (g) Rayonix MX170-HS detector mounted at the ID09 beamline at ESRF (Wulff *et al.*, 2002). (h) Both dimensions (vertical and horizontal) are the same. (i) Parameters as close as possible to mimic the CEA Reflex emulsion films (Helliwell *et al.*, 1989). (j) Limiting values estimated from the λ curve plots.

Table 2
Refinement of selected parameters for the studied Laue data sets.

d is expressed in mm, and *x*₀ and *y*₀ in native detector pixel coordinates (see the supporting information). In certain cases the errors are so small that a non-standard notation for values and their e.s.d.s is used.

Data set	Initial values			Final values		
	<i>d</i>	<i>x</i> ₀	<i>y</i> ₀	<i>d</i>	<i>x</i> ₀	<i>y</i> ₀
simAgCu ^a	70.0	19540.0	19730.0	65.00 ± 8 × 10 ⁻⁵	19540.00 ± 1 × 10 ⁻⁵	19730.00 ± 2 × 10 ⁻⁵
	65.0	19200.0	19730.0	65.00 ± 8 × 10 ⁻⁵	19540.00 ± 1 × 10 ⁻⁵	19730.00 ± 2 × 10 ⁻⁵
	80.0	19200.0	19850.0	65.00 ± 8 × 10 ⁻⁵	19540.00 ± 1 × 10 ⁻⁵	19730.00 ± 1 × 10 ⁻⁵
simPeaL ^b	105.0	1215.0	1286.0	95.00 ± 3 × 10 ⁻⁵	1215.00 ± 1 × 10 ⁻⁶	1286.00 ± 1 × 10 ⁻⁶
	95.0	1240.0	1286.0	95.00 ± 3 × 10 ⁻⁵	1215.00 ± 1 × 10 ⁻⁶	1286.00 ± 1 × 10 ⁻⁶
	100.0	1240.0	1250.0	95.00 ± 3 × 10 ⁻⁵	1215.00 ± 1 × 10 ⁻⁶	1286.00 ± 1 × 10 ⁻⁶
expCuDppe ^c	120.0	19860.0	19640.0	100.80 (7)	19860.174 (5)	19650.013 (7)
	100.0	19500.0	19640.0	100.80 (7)	19860.174 (5)	19650.013 (7)
	120.0	19500.0	19500.0	100.80 (7)	19860.177 (5)	19650.020 (7)
expCuDmdpp	50.0	1910.0	1924.0	47.25 (2)	19040.1507 (9)	19230.046 (1)
	55.0	1900.0	1900.0	47.25 (2)	19040.1497 (9)	19230.044 (1)
	70.0	1920.0	1950.0	47.25 (2)	19040.1504 (9)	19230.047 (1)

(a) Target values for **simAgCu**: *d* = 65.0 mm, *x*₀ = 19540.0 pixels, *y*₀ = 19730.0 pixels (Table 1). (b) Target values for **simPeaL**: *d* = 95.0 mm, *x*₀ = 1215.0 pixels, *y*₀ = 1286.0 pixels (Table 1). (c) Target values for **expCuDppe**: *d* = 100.0 mm, *x*₀ = 19860.0 pixels, *y*₀ = 19640.0 pixels (Table 1).

al. without any IM refinement. As such, this data set presented a challenge for our software. The final step of the indexing method is to cluster the points in the Euler-angle space, each representing a single determined orientation matrix (the method is based on testing multiple orientation matrices). The final orientation matrix is considered to be an average of all matrices belonging to a single cluster. For the ESRF data, the detector distance was initially set and calibrated to 50 mm. The detector centre was not directly measured, but instead it was assumed to be very close to the centre of the X-ray beamstop shadow area (*x*₀ = 1910 pixels, *y*₀ = 1924 pixels; see the supporting information). However, starting from these values, the procedure yielded only ten clusters for **expCuDmdpp**. This rather poor determination of the orientation matrix considerably hampered further data processing. We ascribe these difficulties to imperfect instrument-model parameters, which tend to drift from their starting positions (properly calibrated initially) over the very long experiment time (*ca* 5 days of constant data collection). The refinement of the IM parameters [final values: *d* = 47.25 (2) mm, *x*₀ = 1904.1507 (9) pixels, *y*₀ = 1923.046 (1) pixels] with our new approach enabled us to find the orientation matrix readily and reliably. The total number of determined clusters increased considerably (to 268), which indicated correct determination of the crystal orientation. It is also worth noting that the refined beam centre stayed in the beamstop shadow area, which constituted additional confirmation of the IM refinement method's validity.

It appears that there are essentially no correlations between the refined parameters. The largest correlation coefficients, which reach only up to 20%, are found for the simulated data sets (*ca* 20% for the *x*₀ – *y*₀ parameter pair and *ca* 18% for *d* – *x*₀, for **simAgCu** and **simPeaL**, respectively). In turn, the values of the correlation coefficients calculated for the experimental data sets do not exceed 6%. Such results can be expected, since in our method changes in the *d*, *x*₀ and *y*₀

parameters have significantly different effects on the positions of the reflections and thus on the computed normalized vectors (a change in d results in the radial movement of reflections – all inwards or outwards – whereas changes in x_0 and y_0 lead to vertical and horizontal shifts of the reflections, respectively). We believe that larger correlations might be found when more elaborate and complex instrument models are implemented (*e.g.* incorporating goniometer angle zeros, detector pitch–roll–yaw misalignment angles *etc.*), or when other physical factors cannot be neglected during the data collection (*e.g.* laser-pulse-induced thermal expansion of a crystal may have a somewhat similar effect on the diffraction pattern as the distance change). These, however, are not considered in this contribution.

Finally, it should be stressed that the main assumption of the method is that the crystal remains fixed during the entire experiment, and thus any irregular movements during the data collection are eliminated. This is most efficiently realized by glueing the crystal to the capillary, which is standard practice for crystals of small molecules. Such sample handling is especially important during time-resolved experiments where the high-power laser hits the sample and thus may change the crystal orientation. For small molecules, where the highest possible accuracy and precision is necessary, it is a crucial issue of the further data processing utilizing the RATIO method. On the other hand, in the case of protein samples, glueing of the crystal to a capillary is often impractical (it has not been done even in the case of PYP, which was successfully analysed with the modified RATIO method; Schotte *et al.*, 2012). As a consequence, here the crystal can move more significantly, which outweighs slight goniometer misalignments. Taking into account the differences in the data processing techniques (protein diffraction patterns are much less sparse), these misalignments are overall less important than the crystal movements. Furthermore, in the limiting case of serial microcrystallography, every crystal yields a single diffraction frame with essentially random orientation. To resolve such cases, different approaches have been developed (Campbell, 1995; Helliwell *et al.*, 1989; Ren *et al.*, 1999; Gevorkov *et al.*, 2020, 2019; Beyerlein *et al.*, 2017; Ginn *et al.*, 2016), but our method is not applicable.

3. Conclusions and summary

A new algorithm to refine the diffractometer instrument model using normalized reciprocal space vectors has been developed and tested for use in the analysis of synchrotron-generated X-ray Laue diffraction data. The method is applicable for data sets in which multiple consecutive frames are recorded for different crystal orientations and no irregular sample movements are present. The method does not need any data other than the diffraction spot positions and frame angular setting angles. It has been proved for both model simulated and experimental data sets that the method provides very good results. The refinement readily converges even when the initial deviations from the target values are rather large. Most importantly, the method allows for deter-

mination of the IM parameters which had been previously unknown or had been known with low accuracy (which significantly hampered the orientation-matrix determination). This constitutes a major improvement in the small-molecule X-ray Laue diffraction processing pipeline. The algorithm is implemented in our new Laue data processing software (Szarejko *et al.*, 2020; Jarzemska *et al.*, 2019). The current version of the program (including the source code), interfaced also with the *LaueUtil* suite (Kalinowski *et al.*, 2011, 2012), is available from the authors upon request (the program code will be available publicly open source shortly).

Acknowledgements

Some of the time-resolved X-ray diffraction experiments were performed at the ID09 beamline of the European Synchrotron Radiation Facility (ESRF), Grenoble, France. The authors thank Robert Henning, Anthony DiChiara and Vukica Šrajer for continuous support of our APS experiments.

Funding information

RK, DS and PŁ acknowledge the SONATA grant (2016/21/D/ST4/03753) of the National Science Centre in Poland for financial support. LEH and PRR are grateful to the Engineering and Physical Sciences Research Council (UK) for funding (grant No. EP/K004956/1). The research also used the resources of the Advanced Photon Source (APS), a US Department of Energy (DOE) Office of Science User Facility operated for the DOE Office of Science by Argonne National Laboratory under contract No. DE-AC02-06CH11357. Use of BioCARS was additionally supported by the National Institute of General Medical Sciences of the National Institutes of Health (NIH) under grant No. R24GM111072 (note: the content is solely the responsibility of the authors and does not necessarily represent the official views of NIH). The time-resolved setup at Sector 14 was funded in part through collaboration with Philip Anfinrud (NIH/NIDDK).

References

- Arvai, A. (2019). *Adxv – A Program to Display X-ray Diffraction Images*, <https://www.scripps.edu/tainer/arvai/adxv.html>.
- Benedict, J. B., Makal, A., Sokolow, J. D., Trzop, E., Scheins, S., Henning, R., Graber, T. & Coppens, P. (2011). *Chem. Commun.* **47**, 1704–1706.
- Beyerlein, K. R., White, T. A., Yefanov, O., Gati, C., Kazantsev, I. G., Nielsen, N. F.-G., Larsen, P. M., Chapman, H. N. & Schmidt, S. (2017). *J. Appl. Cryst.* **50**, 1075–1083.
- Borgstahl, G. E. O., Williams, D. R. & Getzoff, E. D. (1995). *Biochemistry*, **34**, 6278–6287.
- Campbell, J. W. (1995). *J. Appl. Cryst.* **28**, 228–236.
- Coppens, P. (2011). *J. Phys. Chem. Lett.* **2**, 616–621.
- Coppens, P. & Fournier, B. (2015). *J. Synchrotron Rad.* **22**, 280–287.
- Coppens, P., Kamiński, R. & Schmökel, M. S. (2010). *Acta Cryst.* **A66**, 626–628.
- Coppens, P., Makal, A., Fournier, B., Jarzemska, K. N., Kamiński, R., Basuroy, K. & Trzop, E. (2017). *Acta Cryst.* **B73**, 23–26.
- Coppens, P., Pitak, M., Gembicky, M., Messerschmidt, M., Scheins, S., Benedict, J., Adachi, S., Sato, T., Nozawa, S., Ichiyonagi, K., Chollet, M. & Koshihara, S. (2009). *J. Synchrotron Rad.* **16**, 226–230.

- Coppens, P., Zhang, L., Thomas, R., Chen, Y., Jarzemska, K., Kaminski, R., Trzop, E. & Fournier, B. (2016). *Phys. Scr.* **91**, 023003.
- Cruickshank, D. W. J., Helliwell, J. R. & Moffat, K. (1987). *Acta Cryst.* **A43**, 656–674.
- Cruickshank, D. W. J., Helliwell, J. R. & Moffat, K. (1991). *Acta Cryst.* **A47**, 352–373.
- Einspahr, H., Parkst, E. H., Sugunall, K., Subramanian, E. & Suddath, F. L. (1986). *J. Biol. Chem.* **261**, 16518–16527.
- Gevorkov, Y., Barty, A., Brehm, W., White, T. A., Tolstikova, A., Wiedorn, M. O., Meents, A., Grigat, R.-R., Chapman, H. N. & Yefanov, O. (2020). *Acta Cryst.* **A76**, 121–131.
- Gevorkov, Y., Yefanov, O., Barty, A., White, T. A., Mariani, V., Brehm, W., Tolstikova, A., Grigat, R.-R. & Chapman, H. N. (2019). *Acta Cryst.* **A75**, 694–704.
- Ginn, H. M., Roedig, P., Kuo, A., Evans, G., Sauter, N. K., Ernst, O. P., Meents, A., Mueller-Werkmeister, H., Miller, R. J. D. & Stuart, D. I. (2016). *Acta Cryst.* **D72**, 956–965.
- Graber, T., Anderson, S., Brewer, H., Chen, Y.-S., Cho, H. S., Dashdorj, N., Henning, R. W., Kosheleva, I., Macha, G., Meron, M., Pahl, R., Ren, Z., Ruan, S., Schotte, F., Šrajcar, V., Viccaro, P. J., Westferro, F., Anfinrud, P. & Moffat, K. (2011). *J. Synchrotron Rad.* **18**, 658–670.
- Hajdu, J., Machin, P. A., Campbell, J. W., Greenhough, T. J., Clifton, I. J., Zurek, S., Gover, S., Johnson, L. N. & Elder, M. (1987). *Nature*, **329**, 178–181.
- Hatcher, L. E. & Raithby, P. R. (2014). *Coord. Chem. Rev.* **277–278**, 69–79.
- Helliwell, J. R., Habash, J., Cruickshank, D. W. J., Harding, M. M., Greenhough, T. J., Campbell, J. W., Clifton, I. J., Elder, M., Machin, P. A., Papiz, M. Z. & Zurek, S. (1989). *J. Appl. Cryst.* **22**, 483–497.
- Jarzemska, K. N., Hapka, M., Kamiński, R., Bury, W., Kutniewska, S. E., Szarejko, D. & Szcześniak, M. M. (2019). *Crystals*, **9**, 36.
- Jarzemska, K. N., Kamiński, R., Dziubek, K. F., Citroni, M., Paliwoda, D., Durka, K., Fanetti, S. & Bini, R. (2018). *Inorg. Chem.* **57**, 8509–8520.
- Jarzemska, K. N., Kamiński, R., Fournier, B., Trzop, E., Sokolow, J. D., Henning, R., Chen, Y. & Coppens, P. (2014). *Inorg. Chem.* **53**, 10594–10601.
- Kalinowski, J. A., Fournier, B., Makal, A. & Coppens, P. (2012). *J. Synchrotron Rad.* **19**, 637–646.
- Kalinowski, J. A., Makal, A. & Coppens, P. (2011). *J. Appl. Cryst.* **44**, 1182–1189.
- Kaminski, R., Benedict, J., Trzop, E., Jarzemska, K., Fournier, B. & Coppens, P. (2014). *Acta Cryst.* **A70**, C775.
- Koshevoy, I. O., Shakirova, J. R., Melnikov, A. S., Haukka, M., Tunik, S. P. & Pakkanen, T. A. (2011). *Dalton Trans.* **40**, 7927–7933.
- Machin, P. (1985). *Laue Photographs Using Synchrotron X-radiation. Report on a Daresbury Synchrotron Radiation PX Users' Meeting and Additions of Work Done Since Then, CCP4 Newsletter on Protein Crystallography*, Vol. 15.
- Makal, A., Benedict, J., Trzop, E., Sokolow, J., Fournier, B., Chen, Y., Kalinowski, J. A., Graber, T., Henning, R. & Coppens, P. (2012). *J. Phys. Chem. A*, **116**, 3359–3365.
- Paciorek, W. A., Meyer, M. & Chapuis, G. (1999). *Acta Cryst.* **A55**, 543–557.
- Ren, Z., Bourgeois, D., Helliwell, J. R., Moffat, K., Šrajcar, V. & Stoddard, B. L. (1999). *J. Synchrotron Rad.* **6**, 891–917.
- Schotte, F., Cho, H. S., Kaila, V. R. I., Kamikubo, H., Dashdorj, N., Henry, E. R., Graber, T. J., Henning, R., Wulff, M., Hummer, G., Kataoka, M. & Anfinrud, P. A. (2012). *Proc. Natl Acad. Sci. USA*, **109**, 19256–19261.
- Šrajcar, V., Crosson, S., Schmidt, M., Key, J., Schotte, F., Anderson, S., Perman, B., Ren, Z., Teng, T., Bourgeois, D., Wulff, M. & Moffat, K. (2000). *J. Synchrotron Rad.* **7**, 236–244.
- Szarejko, D., Kamiński, R., Łaski, P. & Jarzemska, K. N. (2020). *J. Synchrotron Rad.* **27**, 405–413.
- Trzop, E., Fournier, B., Jarzemska, K., Sokolow, J., Kaminski, R., Benedict, J., Chen, Y., Henning, R. & Coppens, P. (2014). *Acta Cryst.* **A70**, C776.
- Vorontsov, I., Pillet, S., Kamiński, R., Schmökel, M. S. & Coppens, P. (2010). *J. Appl. Cryst.* **43**, 1129–1130.
- Vorontsov, I. I., Graber, T., Kovalevsky, A. Y., Novozhilova, I. V., Gembicky, M., Chen, Y.-S. & Coppens, P. (2009). *J. Am. Chem. Soc.* **131**, 6566–6573.
- Wulff, M., Plech, A., Eybert, L., Randler, R., Schotte, F. & Anfinrud, P. (2002). *Faraday Disc.* **122**, 13–26.